Final Draft
of the original manuscript:

Madia, M.; Baretta, S.; Zerbst, U.:
An investigation on the influence of rotary bending and press fitting on stress intensity factors and fatigue crack growth in railway axles
In: Engineering Fracture Mechanics (2007) Elsevier

DOI: 10.1016/j.engfracmech.2007.08.015

AN INVESTIGATION ON THE INFLUENCE OF ROTARY BENDING AND PRESS FITTING ON SIF SOLUTIONS AND FATIGUE CRACK GROWTH IN RAILWAY AXLES

M. Madia[a*], S. Beretta[a] and U. Zerbst[b]

[a] *Department of Mechanical Engineering, Politecnico di Milano, I-20156 Milano, Italy*
[b] *Institute for Materials Research, GKSS Research Centre, Max-Planck-Str. 1, D- 21502 Geesthacht, Germany*

Abstract

The present paper summarizes the results of fatigue crack growth investigations on a hollow railway axle which were performed as a joint research project between the Politecnico di Milano, Italy, and the GKSS Research Centre Geesthacht, Germany, in the frame of an ESIS-TC24 activity. Since no analytical K factors (SIF) solutions for semi-elliptical surface cracks in the S-transitions of railway axles were available, the first step in the research was to generate them for both reverse and rotary bending. The results were then used to investigate the effects of rotary bending and of the press fits at the wheel and gear on the fatigue crack growth and residual lifetime so as to provide essential input information for setting up inspection intervals. It was found that the effect of rotary bending, although existent, was rather moderate whereas the press fits had a large and detrimental effect.

Keywords: Railway axles; Press fitting; Rotary bending; Crack propagation; Damage tolerance

1. Introduction

Railway axles were investigated at the very beginning of fatigue research and design. Since the early work of Wöhler in 1871, technologies and analytical tools have been developed, which ensure that the number of in-service failures of these components is very small today [1,2].

[*] Corresponding author: Tel.: +39 02 2399 8246; fax: +39 02 2399 8202
E-mail address: mauro.madia@polimi.it (M. Madia).

Nevertheless, with the emergence of high speed trains, more detailed analyses are needed in order to improve predictions of residual lifetime and to optimize the inspection regime for railway components. A particular focus is put on damage tolerance analyses, which use the typical tools of fracture mechanics, fatigue crack growth and statistics [3-6]. There is a wide range of SIF solutions for cracks in round bars and pipes subjected to different load conditions [7-10], however, few of these refer to cracks at notches [11] and almost no solutions are available which cover the geometry and dimensions of hollow railway axles. However, specific SIF solutions for railway axles, including the geometrical transitions, are needed [12] because the transitions, together with the press seats, represent the typical positions of crack initiation [3,4]. Two important aspects were taken into account with regards to SIF values of railway axles: (a) the axles are subjected to rotary bending and, (b) the geometrical transitions are at the press fits of either the wheels or gears, or adjacent to them.

The effect of rotary bending can easily be illustrated by the scheme presented in Fig. 1.a. If one considers the bending axis fixed (the load is always acting in the vertical plane), the relative position of the surface crack changes due to the rotation of the axle. The consequence is that the SIF value at crack tip B (K_B) is higher in rotary bending than in reverse bending, reaching a maximum value at the rotation angle $\theta_0 \neq 0$ with θ_0 dependent on the crack size.

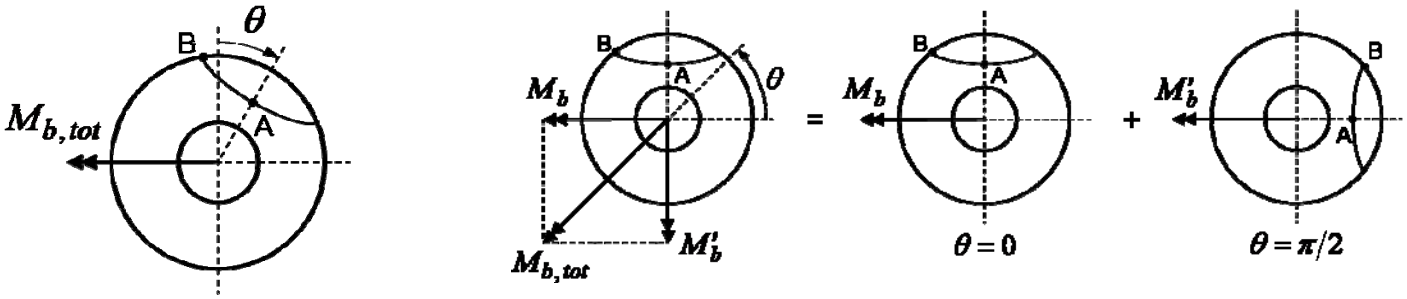

a) b)

Fig. 1. Scheme of the rotation of the axle: the crack changes its position with respect to the fixed applied bending moment $M_{b,tot}$ (a) which can be modelled as the superposition of M_b (crack at $\theta = 0$) and M_b' (crack at $\theta = \pi/2$) (b).

The only analytical approach to this problem was presented by Carpinteri et al. [8] who obtained the analytical expression $K_B(\theta)$ combining SIF solutions for reverse bending at $\theta = 0$ and $\theta = \pi/2$ (Fig. 1.b). The effects of a higher SIF at the surface crack tip B were approved by crack growth investigations. During the initial phase of propagation, there is a negligible difference between reverse and rotary bending, but beyond a crack depth of about $a/D = 0.15$ the K_B values become significantly higher in rotary bending. This leads to flattening of the crack in rotary bend loading as is also confirmed by experimental results [13]. Whereas the effect is less pronounced for the smooth parts of the axle [14], severe mistakes can be made when the rotary bending effect is neglected for cracks originating at the geometrical transition since it is additionally magnified by the local stress distribution due to the notch [15,16].

The effect of press fits on SIF was briefly discussed by Beretta et al. [17] based on the results of finite element simulations on a bending loaded railway axle. The longitudinal stress field in the region next to the press fit, if compared with the field without press fit, shows significant differences. The maximum positive stress is higher in the case of wheel press fit and the stress field is no longer symmetric. That means that a small crack in that region is subjected not only to the bending stresses due to the applied load, but also to the stresses induced by the press fits. Note that Zerbst and Schödel [18], in contrast, found a beneficial effect of the press fit on the residual lifetime in fatigue cracks initiated in the press seat itself.

In order to quantify the influence of rotary bending and press fitting on the stress intensity factor, this paper presents a series of SIF solutions for cracks at the S-transition of a real locomotive axle under rotary bending considering both wheel and gear press fits.

2. Crack configuration and FE modelling

2.1 Geometry

The analyses were carried out on a driving axle of a high speed train, the main geometrical features of which (see Fig. 2) follow specific normative requirements [12]. It is a hollow axle with press fits for the gear and wheel. Fig. 2.a shows the most relevant section of the axle for fatigue design. The transition between the

axle body and the gear seat is called T-notch (Fig. 2.b), the groove between the gear seat and the wheel seat is the S-transition (Fig. 2.c).

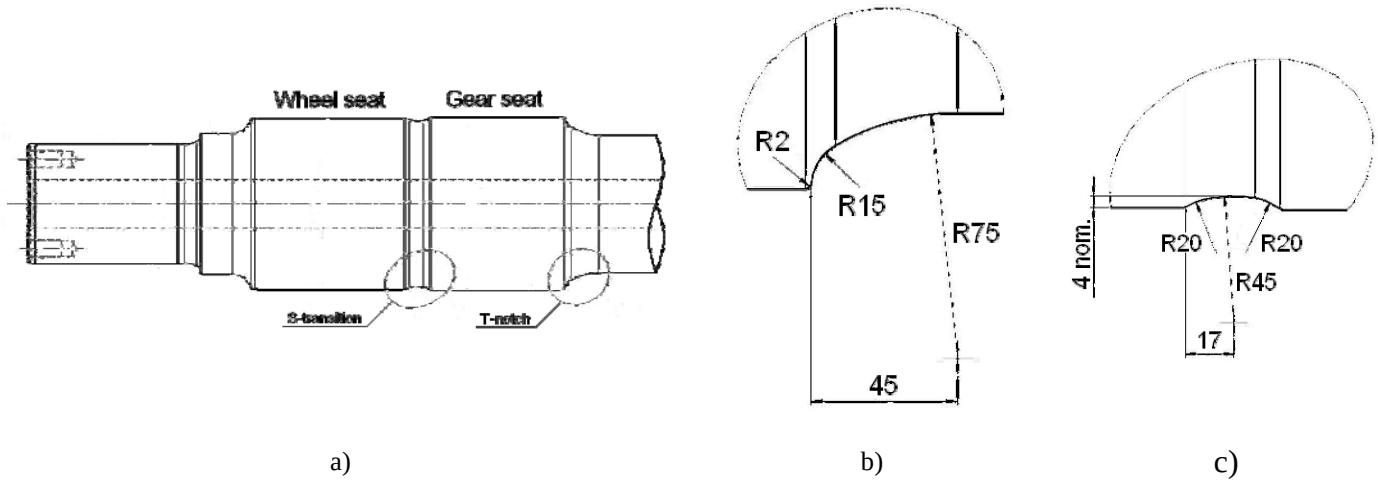

a) b) c)

Fig. 2. Geometry of the hollow driving axle: a) gear and wheel seat; b) dimensions of the T-notch; c) dimensions of the S-transition.

The geometrical transitions between the wheel seats and bearing journals, as well as the T-notch, are not investigated in the present work since some SIF solutions were already presented for these transitions [17]. The axle was analysed using the FE method in order to determine the stress field and the SIFs for the cracks modelled at the S-transition; to be more specific the commercial software ABAQUS® [19] was used.

In components such as railway axles, crack propagation usually starts from surface defects or inclusions which can be modelled as semi-elliptical and semi-circular flaws, respectively [20]. Note, however, that damage tolerance does not deal with small defects but with defects large enough to be detected in non-destructive inspection. Depending on the techniques applied these “initial” cracks are in the order of 2 mm in depth. What is important in that context is not the smallest defect which could be found, but the largest defect that could escape detection under service conditions. Surface cracks in railway axles usually have a semi-elliptical shape (e.g. [3,13,21]). An example from a failure case is shown in Fig. 3.a.

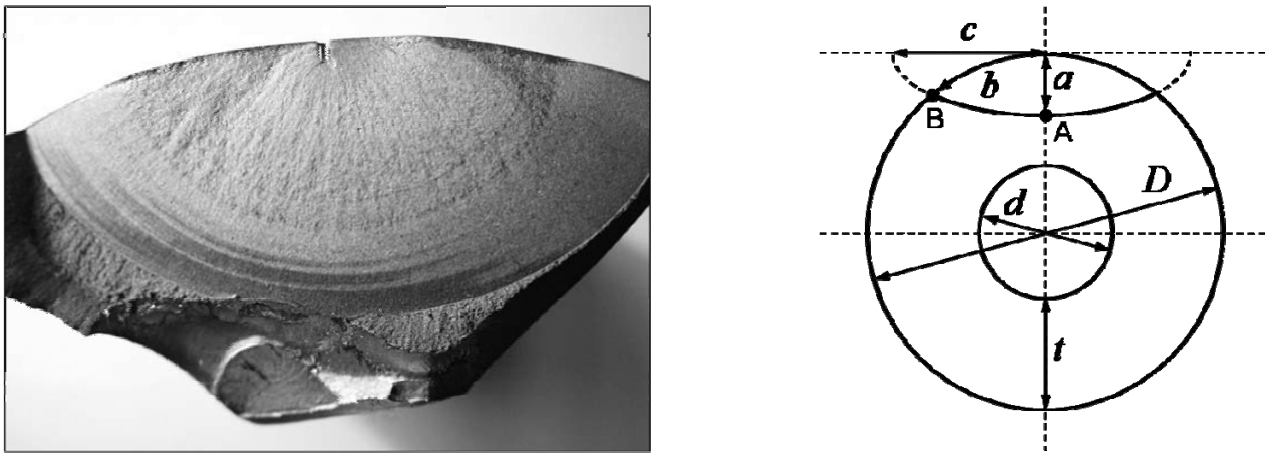

a) b)

Fig. 3. Crack propagation in a full scale test (a) [21] and crack model adopted in the numerical analysis (b).

During propagation the crack geometry, i.e., its depth to surface length ratio a/c changes with increasing aspect ratio a/t (for the definition of this terms see Fig. 3b) but its basic shape stays semi-elliptical such as shown in a number of experiments. Within the present analysis K factor solutions were obtained for various a/c and a/t ratios (see Table 1).

Table 1
a/c and a/t ratios for which SIF solutions have been determined by finite elements

a/t	a/c
0.02 - 0.1 - 0.4 - 0.7	0.2 - 0.35 - 0.5 - 0.75 - 1.0

2.2 The FE model

SIF solutions were obtained on the basis of J-integral determination using the method of virtual crack extension and domain integrals [19]. The most suitable strategy for this purpose was to apply a non-conform meshing technique in order to refine the mesh surrounding the crack front directly in the global model.
The continuity of the stress-strain field at the boundary of each sub-region was ensured using the tie contact definition permitted by ABAQUS [19] to bond together the adjacent regions and matching the mesh pattern of the surfaces involved in the tie contact as much as possible.

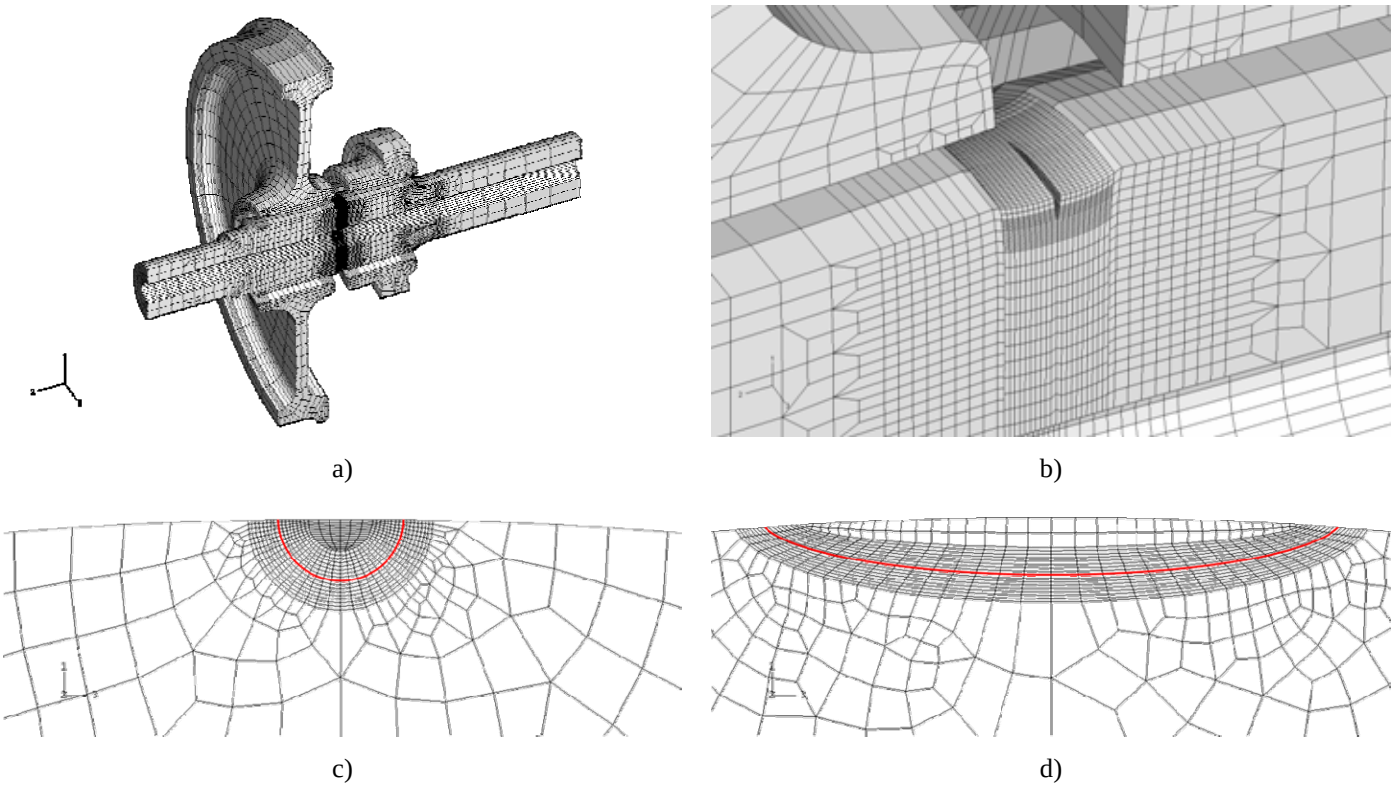

Fig. 4. Finite element model: a) global view of the longitudinal section of the axle; b) crack at the S-transition; c) detail of the mesh for a crack with $a/t = 0.02$ and $a/c = 1.0$; d) detail of the mesh for a crack with $a/t = 0.02$ and $a/c = 0.2$.

Fig. 4 shows a typical finite element model used during the fracture mechanics analysis. The mesh was refined in the proximity of the transition regions, whereas a quite coarse mesh was adopted elsewhere. The principle of the non-conform meshing is illustrated in Fig. 4b (crack at the S-transition). The technique was particularly suited for the present purpose since the mesh in the section containing the crack was much finer than the mesh in the surrounding regions. Fig. 4.c and Fig. 4.d show the mesh refinement of the crack front region.

A critical point in the FE modelling was the correct attachment of the wheel (and gear) to the axle: the convergence of the forces at the contact points is a particularly delicate operation. In order to assure convergence and to reduce the computational effort, careful meshing of the contact surfaces is necessary. Suitable numerical tools have then to be adopted for the contact pair. Although there were a number of alternatives**,** the interference fit method [19] was used to model the fittings in the present study. This kind of procedure is based on a master-slave contact type, the main parameter of which is a user-defined specific

radial interference ν. A clearance value equal to ν is introduced between the contact surfaces. Note that only normal contact is created in that way.

The behaviour in tangential direction is based on the classical Coulomb approach, i.e. the maximum allowable shear stresses ($\tau_{\max,i}$) are related to the contact pressure (p_i) due to the press fit between the bodies in contact. This is realised using a friction coefficient (μ). The subscript i refer to point wise determined $\tau_{\max,i} = \mu \cdot p_i$ of the contact surfaces [19]. Note that the friction coefficient μ was considered as a constant with a value of 0.6.

Automatic contact controls [19] was adopted to improve the convergence.

The element type used in the analysis was the solid isoparametric hexaedra with 8 nodes and full integration [19]. It was chosen subsequent to a sensitivity analysis performed with different element types, because the full integration linear hexaedra was found to yield the best accuracy for problems combining both contact and fracture mechanics, while providing acceptable computational effort.

A crucial issue of the analyses were the boundary conditions. At the beginning, the wheel and the gear were not fitted to the axle which resulted in convergence problems. On the other hand it was not possible to make each body isostatic because otherwise the assembly would have been over-constrained when the press fit was completed. The problem was solved with a numerical trick: the analysis was split into two steps (first step: interference fit, then loading) and spring elements were used for stabilizing the solution. The scheme of the load and boundary conditions for both steps is presented in Fig. 5. Fig. 5.a shows the arrangement of the spring elements. Taking advantage of the symmetry conditions, the axle is constrained by two springs acting in directions 1 and 3; the wheel and the gear are constrained by springs in three directions. The stiffness of the spring elements was set to 1 N/mm which is a value without physical meaning. Fig. 5.b represents the loading step, all spring elements were deactivated and replaced by boundaries designed in order to make the assembly isostatic. In addition, the vertical load was applied at the middle plane of the bearing journal. This configuration was chosen in order to assure a constant bending moment at the axle body.

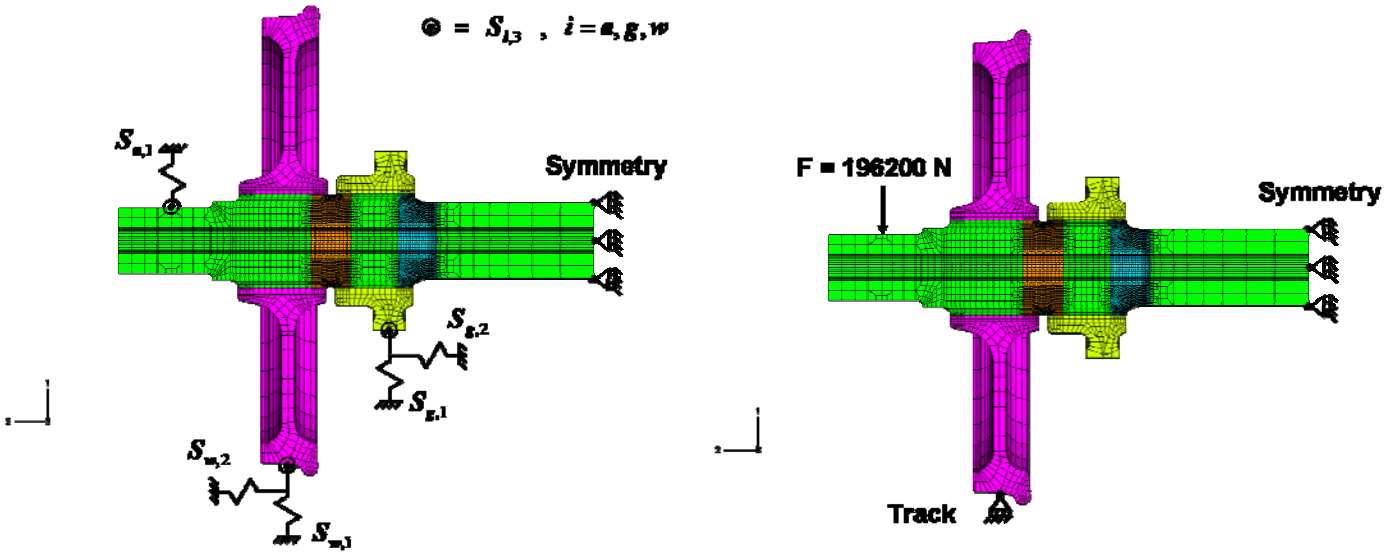

a) b)

Fig. 5. Scheme of the load and boundary conditions in the interference fit step (a) and in the load step (b).

3. Stress analysis

The first step in the analysis dealt with setting up the numerical parameters in order to achieve the stability of the solution combined with an acceptable computation time, no cracks were modelled at this stage. One issue in question concerned the choice of the optimum numerical procedure which should be applied to the press fits. Of particular interest was the question of whether it would be possible to apply the procedure simultaneously to both the wheel and gear press fits or if two subsequent steps were necessary. For answering these questions two simulations were performed in a pre-analysis. The interference value $2\nu = 280$ μm and the friction coefficient $\mu = 0.6$ were chosen in accordance with the common standards [12] and to previous experimental and numerical work [17]. The longitudinal stress path across the thickness at the transition was chosen as an index for comparing the variations.

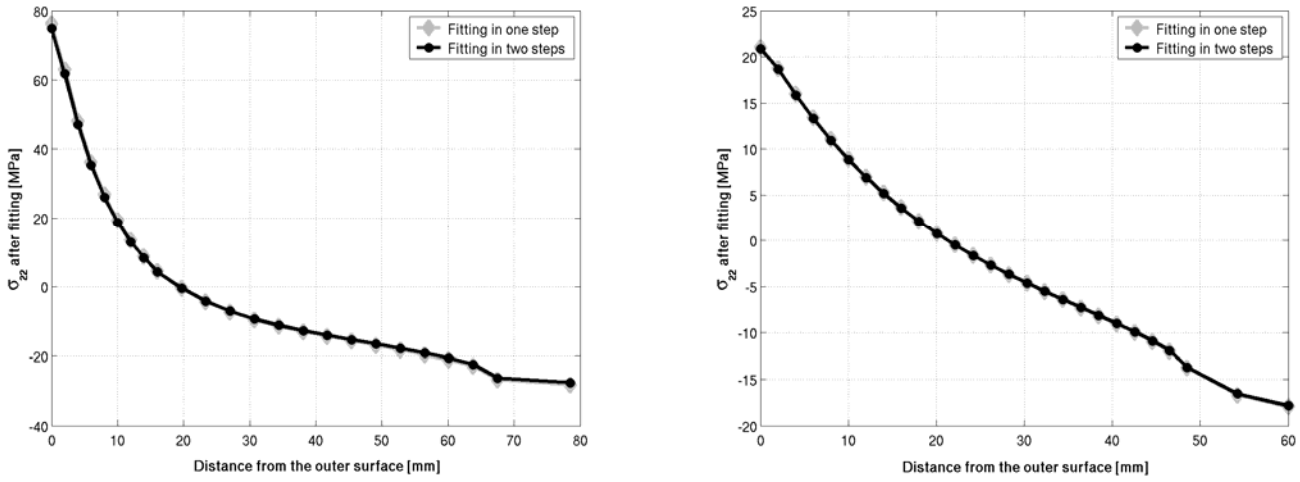

a) b)

Fig. 6. Longitudinal stress path across the thickness for the one and two step analyses: a) results at the S-transition; b) results at the T-notch.

The results of Fig. 6 show that there is no significant difference between the two procedures in terms of stress paths, however, there is a huge difference in terms of computation time (2:3), which clearly speaks in favour of the one-step-technique.

A further important conclusion which can be drawn from Fig. 6 is that the stress values are much higher at the S-transition (Fig. 6.a) than at the T-notch (Fig. 6.b). In addition, a steeper stress gradient across the thickness can be found near the outer surface. More generally, it can be stated that the procedure for applying the press fit gives higher stresses for the S-transition than for the T notch, even though the press fits induce positive longitudinal stresses up to about 20 mm from the outer surface at both notches.

This phenomenon can be illustrated by the resulting deformation and stress fields at the longitudinal symmetry plane (Figs. 7.a and 7.b). Due to the press fit, the wheel and the gear “squeeze” the axle under their seats (Fig. 7.a) and “stretch” the surrounding regions. The corresponding longitudinal stress field is represented by the contours given in Fig. 7.b.

As a consequence, a potential crack at the geometrical transition is loaded by the stress field from applied bending moment and another stress field from the press fit. It’s necessary to take into account both components. The resulting longitudinal stress path in Fig. 7.c is obtained by superposition of both the

effects, i.e. the stress field is magnified by the positive press fit stresses and lowered by the negative ones (Fig. 7.d).

On the right hand side of Fig. 7.d it can also be seen that the stress field is not symmetric anymore. The press fit effect can be considered as a mean stress effect similar to a residual stress effect: it plays an important role mostly in the propagation of a potential crack at the surface of the axle.

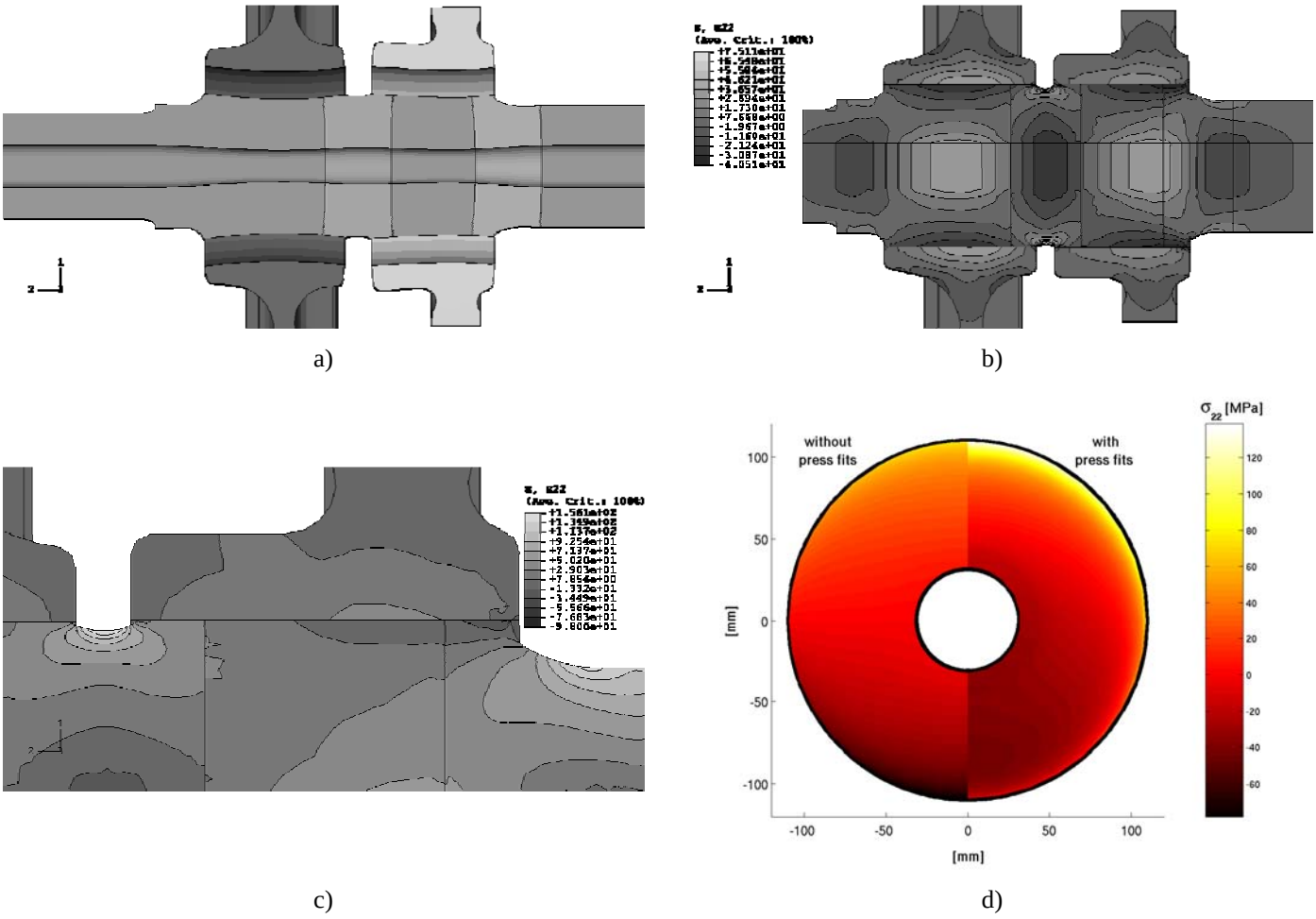

Fig. 7. Stress distribution in the axle: a) the deformed shape (deformation magnification with a scale factor set to 300); b) longitudinal stress field induced by the press fits; c) longitudinal stress field at the notches after the loading step; d) comparison between a simulation performed taking into account the press fitting effect (right hand side) and a simulation with simple bending moment (left hand side).

4. F-factors determination

The *J*-integral was determined for six contours at the crack tip, even in cases where stabilised values were obtained from the third contour upwards (Fig. 8). The path independence of the *J*-integral is an index of the

good quality and reliability of the mesh refinement because of which even a rather coarse mesh is able to assure reliable *J*-integral values, as a number of authors have stated before [22].

Fig. 8 shows that the K_{II} (Fig. 8.b) and K_{III} (Fig. 8.c) values are much lower than K_I (Fig. 8.a). This is also the case for other crack geometries. Therefore the mode II and mode III components were neglected in the following analysis.

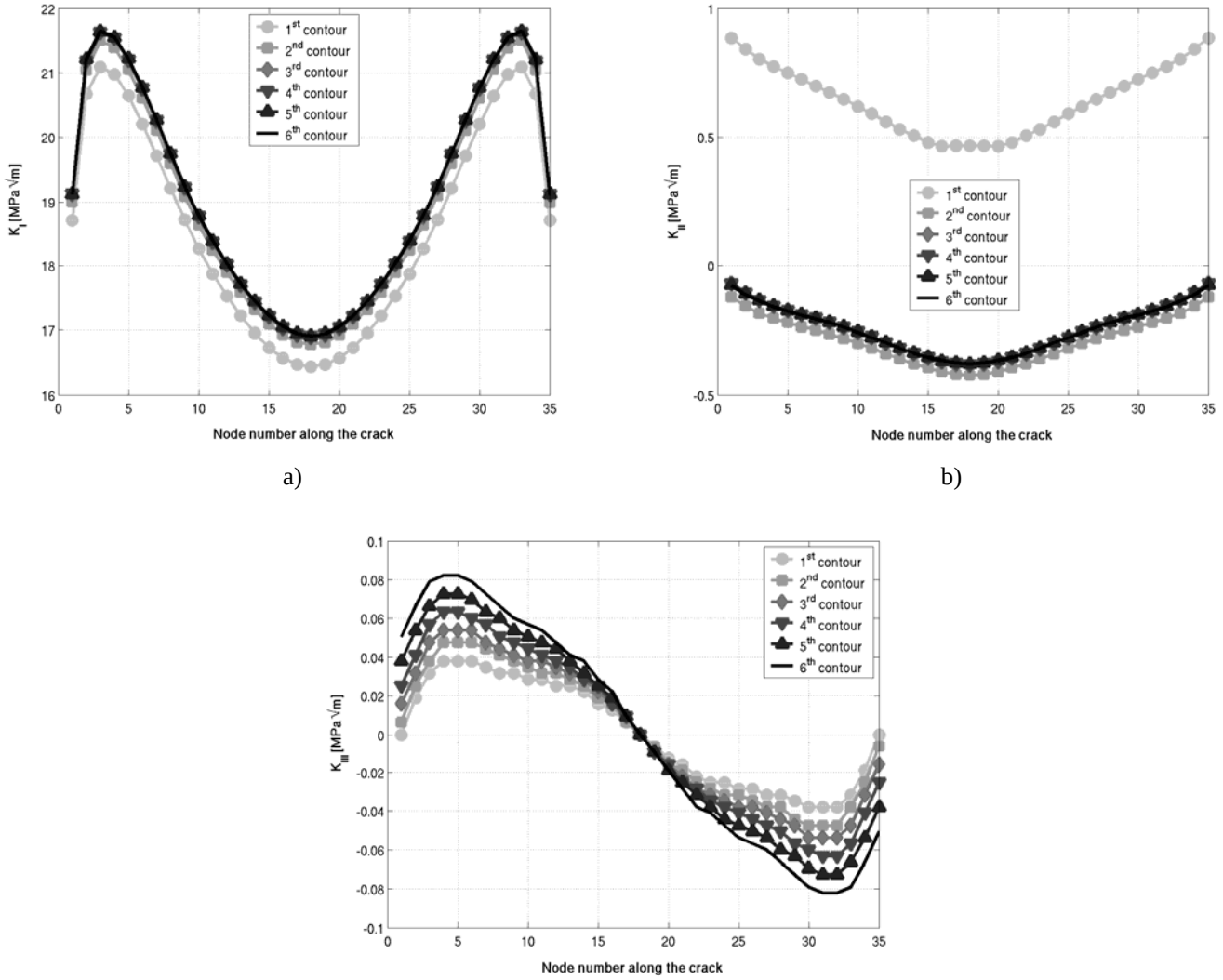

a) b)

c)

Fig. 8. Diagram of the K values along the crack tip for a crack with $a/t = 0.4$ and $a/c = 0.2$. The values of K_{II} (b) and K_{III} (c) are much lower than those of K_I (a).

According to Carpinteri, in order to address the problem of rotary bending, it is necessary to simulate cracks with the axle rotated by $\pi/2$. This can be explained by looking at Carpinteri's approach to SIF under rotary bending [8] (see Fig. 3.b):

$$K_A = (\tilde{F}_A \cdot S_{nom} \cdot \sqrt{\pi \cdot a}) \cdot \cos \vartheta \tag{1}$$

$$K_B = (\tilde{F}_B \cdot S_{nom} \cdot \sqrt{\pi \cdot a}) \cdot \cos \vartheta + (\tilde{F}'_B \cdot S_{nom} \cdot \sqrt{\pi \cdot a}) \cdot \sin \vartheta \tag{2}$$

where $\tilde{F}_A = \tilde{K}_A / \left(\tilde{S}_{nom} \cdot \sqrt{\pi \cdot a}\right)$, $\tilde{F}_B = \tilde{K}_B / \left(\tilde{S}_{nom} \cdot \sqrt{\pi \cdot a}\right)$ and $\tilde{F}'_B = \tilde{K}'_B / \left(\tilde{S}_{nom} \cdot \sqrt{\pi \cdot a}\right)$ are the shape functions related to the SIF values ($\tilde{K}$) for a given nominal stress ($\tilde{S}_{nom}$). The SIF values are functions of the rotation angle ϑ of the axle, the crack depth a and the applied nominal stress S_{nom}. The index (´) in Eq. (2) denotes that the K and F values have been obtained by simulations of the axle turned by $\pi/2$. As stated above, the maximum value for K_A is not affected by rotary bending, whereas it is possible to demonstrate that K_B reaches its maximum value at a turning angle $\vartheta_{B,\max} = arctg\left(\tilde{F}'_B / \tilde{F}_B\right) = arctg\left(\tilde{K}'_B / \tilde{K}_B\right)$.

Eqs. (1) and (2) were compared with the results from FE simulations using the rotary bending mode.

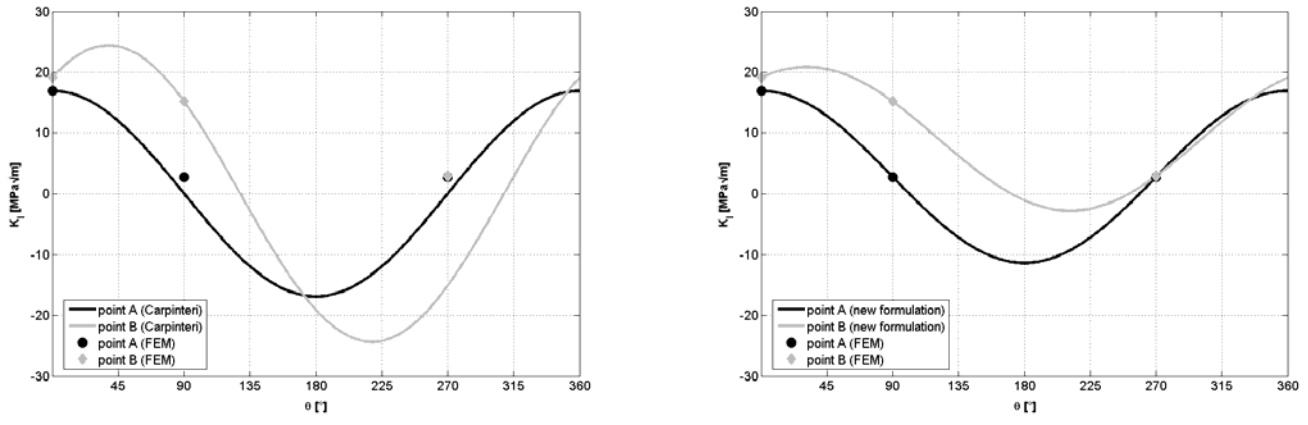

a) b)

Fig. 9. Comparison between the analytical solutions and the FE results for SIF at the crack tips A and B of a crack with $a/t = 0.4$ and $a/c = 0.2$: a) Carpinteri's approach does not match the FE data; b) the new method presented in this paper is able to reproduce the SIF behaviour by taking into account the effect of the press fits.

The results presented in Fig. 9.a show that Carpinteri's superposition method did not match the SIF values obtained by the FE simulations of the present study. The reason for the discrepancy is simply that Carpinteri's approach does not take into account the effect of residual stresses induced by the press fits (§ 3). In terms of fracture mechanics, the press fit induced mean stresses which can be taken into account by introducing a mean SIF, $\overline{K}$, into the original analytical formulation by Carpinteri:

$$K_A = (\tilde{K}_A - \overline{K}_A) \cdot \cos\vartheta + \overline{K}_A \tag{3}$$

$$K_B = (\tilde{K}_B - \overline{K}_B) \cdot \cos\vartheta + (\tilde{K}'_B - \overline{K}_B) \cdot \sin\vartheta + \overline{K}_B \tag{4}$$

The introduction of the new parameter requires an additional equation in order to find the final expressions for the SIF at the crack tips. If we consider K_A , we can state that as $K_A = \tilde{K}'_A$ for $\vartheta = \pi/2$, the following expression can be obtained by substitution in Eq.(3):

$$\overline{K}_A = \tilde{K}'_A \tag{5}$$

The expression for $\overline{K}_B$ is obtained by introducing $K_B = \tilde{K}''_B$ in Eq. (4) for $\vartheta = -\pi/2$:

$$\overline{K}_B = \left(\tilde{K}'_B + \tilde{K}''_B\right)/2 \tag{6}$$

The results of the new formula match perfectly with the SIF values from the FE simulations (Fig. 9.b).

A comparison of the results shown in Figs. 9.a and 9.b reveals that further conclusions can be made. Fig. 9 shows that Carpinteri's approach overestimates both ΔK_A and ΔK_B. A difference was also found for the R values on the basis of K. The assumption of a symmetric load cycle ($R = -1$) proves to be wrong in light of the new formulation, the example presented in Fig. 9.b clearly states that $|K_{\min}| \neq |K_{\max}|$.

How does the presence of the press fit affect fatigue crack propagation? In Fig. 10 it is shown that there is no effect on ΔK. There is, however, a pronounced effect on the effective R values ($R = K_{\min}/K_{\max}$) at the crack tips since the residual stresses induced by the press fits strongly effect $\overline{K}_A$ and $\overline{K}_B$.

Furthermore, a FE analysis carried out with tied connections [18] for the pairs axle-wheel and axle-gear, shows that the resulting SIF calculated with Eq. (4) is exactly the one caused by the press fits minus the effect of $\overline{K}_B$ (Fig. 10).

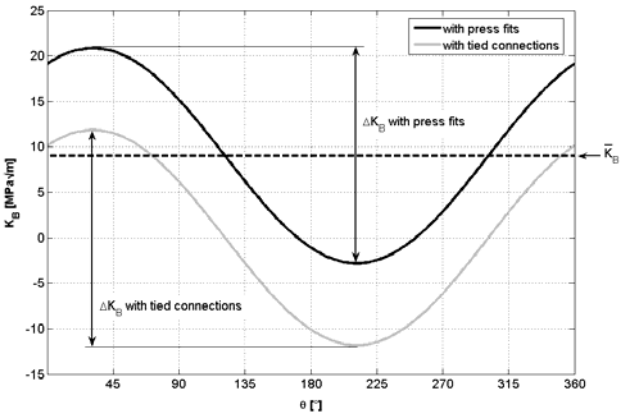

Fig. 10. Influence of the press fits on crack tip loading during crack growth: no difference exists in terms of ΔK in comparison with the SIF solutions obtained with tied connections, the different mean value is, however, taken into account by the stress ratio R.

Note that the stress ratio is a function of the crack geometry and aspect ratio a/c and a/t:

$$R = f\left(a/t, a/c\right) \tag{7}$$

Based on $R = K_{\min}/K_{\max}$, it is possible to find expressions for R at the crack tips A and B:

$$R_A = \frac{2 \cdot \tilde{K}'_A - \tilde{K}_A}{\tilde{K}_A} \tag{8}$$

$$R_B = \frac{\tilde{K}'_B + \tilde{K}''_B - K_{B,\max}}{K_{B,\max}} \tag{9}$$

Using the present approach it is possible to determine both K and R for both crack tips from tabled values (see Table 2).

Table 2
F-factors ($F_A = K_A \big/ \left(\tilde{S}_{nom} \cdot \sqrt{\pi \cdot a} \right)$ and $F_{B,\max} = K_{B,\max} \big/ \left(\tilde{S}_{nom} \cdot \sqrt{\pi \cdot a} \right)$, with K values according to Eqs. (3) and (4)) and stress ratios (Eqs. (8) and (9)) considering the rotary bending effect and the press fit residual stress profile

a/t	a/c	F_A	$F_{B,\max}$	R_A	R_B
0.020	0.200	1.428	0.716	-0.042	-0.012
0.020	0.350	1.324	0.875	-0.043	-0.013
0.020	0.500	1.224	0.985	-0.044	-0.014
0.020	0.750	1.060	1.065	-0.046	-0.014
0.020	1.000	0.919	1.079	-0.048	-0.015
0.102	0.200	1.136	0.721	-0.207	-0.047
0.102	0.350	1.064	0.818	-0.211	-0.056
0.102	0.500	0.981	0.891	-0.218	-0.059
0.102	0.750	0.853	0.968	-0.230	-0.059
0.102	1.000	0.740	0.982	-0.243	-0.058
0.407	0.200	0.809	0.676	-0.673	-0.135
0.407	0.350	0.761	0.765	-0.692	-0.158
0.407	0.500	0.699	0.817	-0.725	-0.165
0.407	0.750	0.587	0.913	-0.797	-0.181
0.407	1.000	0.492	0.928	-0.879	-0.181
0.712	0.200	0.763	0.826	-0.954	-0.250
0.712	0.350	0.717	0.865	-0.988	-0.260
0.712	0.500	0.653	0.909	-1.047	-0.276
0.712	0.750	0.527	0.979	-1.209	-0.298
0.712	1.000	0.417	0.969	-1.439	-0.300

5. Crack propagation and residual lifetime estimation

The residual lifetime analyses focused on the influence of three parameters: (a) the presence of the press fits, (b) rotary bending and (c) the choice of the initial crack shape. The aim of the present work was to investigate the effect of these factors rather than to provide residual lifetimes under realistic load spectra. This being said, a constant maximum amplitude load of 133 MPa (which represents the most detrimental load condition for the axle [12]) was chosen.

Another limitation was that the crack propagation was simulated only up to a crack depth of 40 mm, referring approximately to half the wall thickness.

5.1 Fatigue crack growth algorithm

It is well known that the choice of the fatigue crack growth algorithm plays a crucial role in life prediction. Even though various algorithms are available in literature, for the present purpose a special approach was developed for crack propagation under constant amplitude loading.

At any stage of crack propagation the crack geometry and aspect ratio, a_i/c_i and a_i/t, are evaluated as the input parameters for the next step. The values for K, ΔK and R at the crack tips A and B are then determined by the analytical approach developed within the present study in conjunction with the tabled shape function values of Table 2.

The $da/dN - \Delta K$ curve, the so-called NASGRO equation (also called Forman-Newman-de Koning equation) [23,24] is used:

$$\frac{da}{dN} = C \cdot \left(\Delta K_{eff}\right)^n \cdot \frac{\left(1 - \frac{\Delta K_{th}}{\Delta K}\right)^p}{\left(1 - \frac{K_{\max}}{K_{crit}}\right)^q} \tag{10}$$

In this equation C, n, p and q are empirical constants, ΔK_{th} is the threshold value for ΔK, $K_{\max}$ and K_{crit} are the maximum and the critical SIF values, respectively. The term ΔK_{eff} is the effective stress intensity factor range and it is described by the equation:

$$\Delta K_{eff} = \left(\frac{1 - f}{1 - R}\right) \cdot \Delta K \tag{11}$$

where f describes the plasticity-induced crack closure effect [25] and R is the stress ratio such as above. Eq. (10) consists of three different terms according to the three different propagation regimes: $C \cdot \left(\Delta K_{eff}\right)^n$ represents the Paris regime, $\left(1 - \Delta K_{th}/\Delta K\right)^p$ is used to describe the regime close to the fatigue threshold and $\left(1 - K_{\max}/K_{crit}\right)^q$ describes the regime up to the critical SIF. Note that the equation is separately applied to

the crack depth and its surface dimension, for the latter case replacing a by b. The R values, calculated on the basis of the local K factors, varied along the crack front.

The crack size and stress ratio dependency of the threshold is expressed as follows:

$$\Delta K_{th} = \Delta K_{th0} \cdot \frac{\sqrt{\frac{a}{a + a_0}}}{\left[\frac{1 - f}{(1 - A_0)\cdot(1 - R)}\right]^{(1 + C_{th}\cdot R)}} \tag{12}$$

with ΔK_{th0} being the threshold SIF range at $R = 0$, a the crack depth and a_0 the El-Haddad parameter. A_0 is a constant used in Newman's equation for f [24], whereas C_{th} is an empirical constant which distinguishes positive (C_{th+}) from negative (C_{th-}) R values. Note that Eq. (12), in general, is valid in the range $-2 \le R \le 0.7$ [24].

The parameters of Table 3 used in the crack growth model (Eq. (10)) and in the threshold expression (Eq. (12)) were derived by fitting experimental data obtained on a mild carbon steel (A1N) common for railway axles. The fatigue crack growth properties of A1N were extensively studied by the Authors (more details about the parameters and the testing procedure can be found in [6,21]).

Table 3
Parameters used in the crack growth model and in threshold expression [6,21]

C	$4.53\cdot10^{-10}$
n	2.09
p	1.3
q	0.001
ΔK_{th0}	7.39
C_{th+}	1.442
C_{th-}	–0.02

5.2 Influence of residual stresses (the " press fit effect")

A set of cracks with different aspect ratios was used to investigate the effect of the press fits on residual lifetime and crack shape evolution. The results presented in Fig. 11 refer to an initially semi-circular crack with an aspect ratio $a/t = 0.05$.

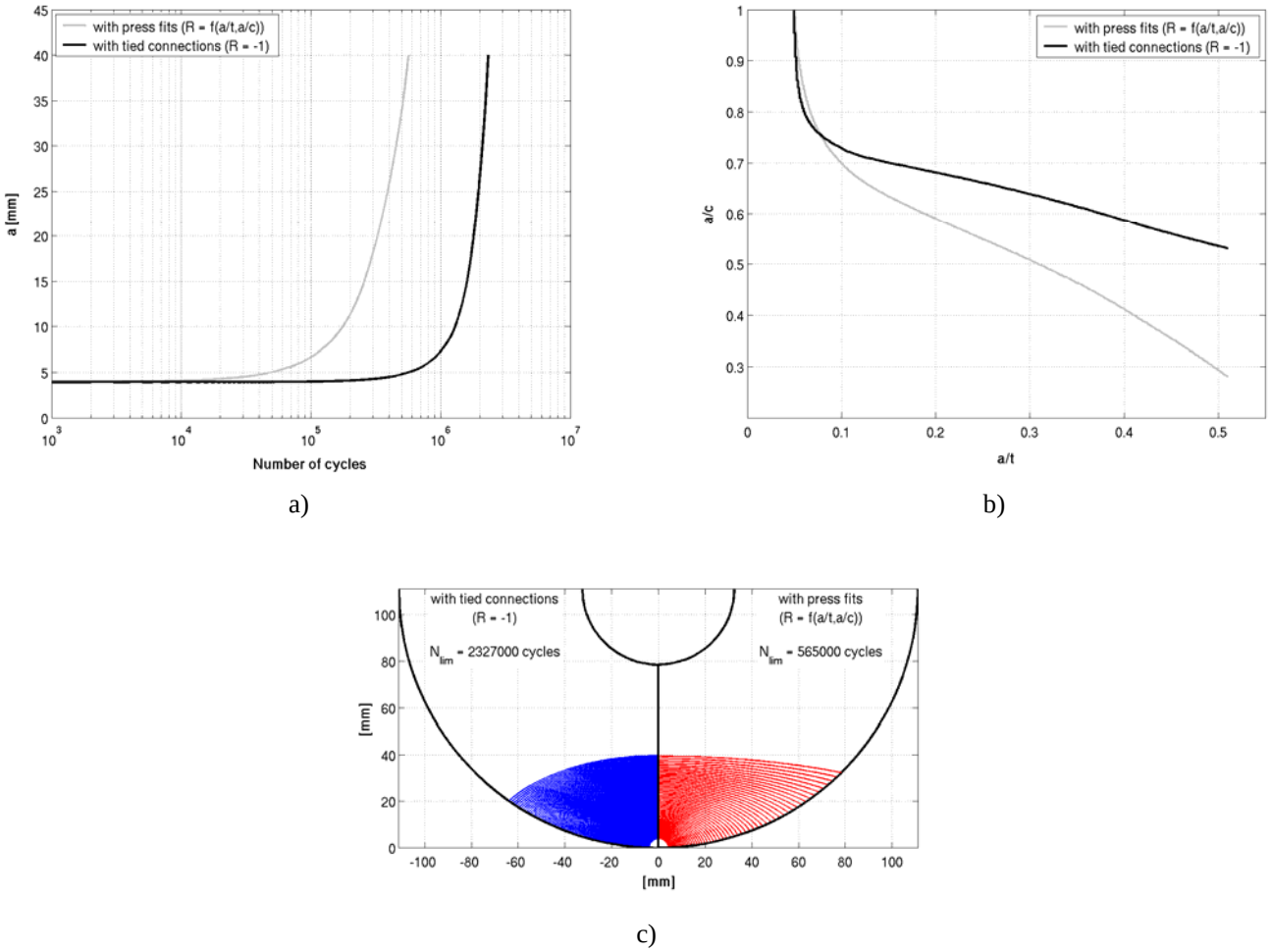

Fig. 11. Influence of the press fits on the propagation of a initially semi-circular crack with $a/t = 0.05$: a) crack extension for the crack tip A; b) crack shape evolution; c) crack contours on the crack plane.

The presence of the press fits was found to be significantly detrimental, i.e. it caused a dramatic reduction in residual lifetime by a factor 4 (Fig. 11.a). This can be explained by an increase in the local R values above the value of -1 caused by the press fits, which resulted in a speeding up of crack propagation at both crack tips. Note that Zerbst and Schödel [18] found a similar though smaller effect for cracks originating in the geometrical transition. However, as mentioned above, they also found a beneficial effect of the press fit for

cracks larger c. 1 mm which originated directly in the press seat. Since the residual lifetime plays an important role in establishing inspection intervals, this is of major concern for any practical application.
The reason for the large difference in residual lifetime is outlined in Figs. 11.b and 11.c: there is a significant difference in crack shape evolution. The press fits cause a speed-up of the crack propagation at crack tip B and, as a consequence, the crack grows shallower.
Note that the difference between the crack propagation rates at tips A and B is even more magnified if the stress gradient due to the fittings is superposed onto the stresses caused by simple bending moment.

5.2 Influence of rotary bending and initial crack shape

The following section aims to present the effects of rotary bending and initial crack shape while taking into account the presence of the press fits.
A number of simulations was performed using initial cracks with different aspect ratios. The results reported in Fig. 12 show the effects of rotary bending and the initial crack shape (a semi-circular crack $a/c = 1$ with $a/t = 0.02$ and a shallow crack $a/c = 0.2$ with $a/t = 0.02$).
The comparison between reverse and rotary bending is based on the initially semi-circular crack.
The results show only a slight difference between reverse and rotary bending in terms of residual lifetime and crack shape evolution. Although there is some reduction in residual lifetime due to the rotary bending effect (Fig. 12.a) this is by far not as detrimental as the effect of the press fits. The difference between reverse and plane bending is less than one percent in the worst case and the effect on crack shape evolution is even more negligible: there is only a bit of a stronger effect during the last stage of the crack propagation ($a/t < 0.25$) (Fig. 12.b). The propagation at the surface crack tip (point B) is slightly faster in the case of rotary bending and the final crack is slightly shallower (Fig. 12.c). Note that Zerbst and Schödel [18] found a slightly larger effect of rotary bending on residual lifetime for cracks at press fits.
The investigation of different initial crack shapes was motivated by the observation that sometimes initial cracks are initiated at more than one site. When these cracks coalescence at an early stage, they form cracks

which are much flatter than semi-circular. In order to address this problem two initial cracks, such as mentioned above, were considered. The initial crack shape was found to be of major influence on residual lifetime prediction. When propagation starts from the shallower crack (Fig. 12.a) a much shorter residual lifetime is the consequence, showing a reduction of about 20% in the example presented. The effect is due to the early stages of crack growth, however, in later stages the crack tends towards the same geometry (Fig. 12.b and Fig. 12.d). A similar phenomenon was already described by other authors both experimentally and numerically [7,8,11,15,16].

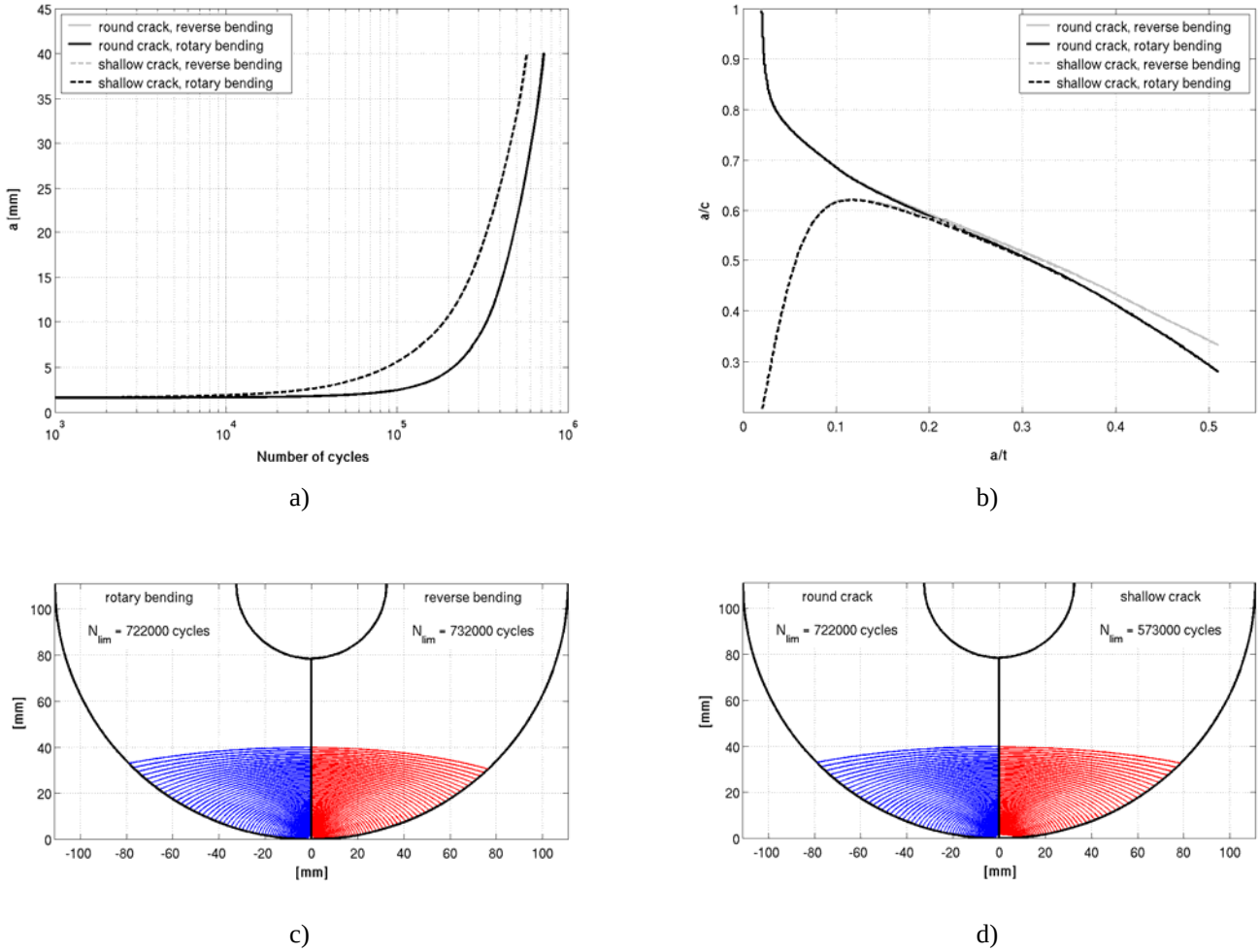

a) b)

c) d)

Fig. 12. Influence of rotary bending and initial crack shape on propagation: a) crack extension for the crack tip A; b) crack shape evolution; c) crack contours onto the crack plane to show the reverse bending vs. rotary bending effect; d) crack contours in case of semi-circular and shallow initial crack.

6. Conclusions

The phenomenon of fatigue crack growth originating from the geometrical transition of a hollow railway axle was investigated. The analysis took into account the effects of rotary bending, the initial crack geometry and the press fits at wheel and gear. The stress intensity factors (SIF), at both the deepest and the surface points of semi-elliptical surface cracks, were established for rotary bending following an approach set out by Carpinteri which had to be modified in order to cover the press fit effect. In the context of these investigations, aspects of the finite element modelling of the press fits have been discussed in detail.

The primary aim of the fatigue crack growth analyses was not to determine realistic residual lifetimes of specific axle geometry but to identify the significance of the effects of the various parameters on lifetime prediction.

It was found that rotary bending, in contrast to reverse bending, reduced the residual lifetime due to the higher loading of the surface points of the crack which also caused a flatter crack shape. The effect was however small and could be covered by a safety factor in practical applications. A more pronounced, but still moderate effect was found in the original crack geometry. Semi-circular cracks are common, however, it happens that many initial cracks develop into one flat crack at an early stage of extension. It is this single crack that then must be used as the initial crack in the analysis. It was shown that such a flat crack causes a reduced residual lifetime of up to 20% compared to a semi-circular crack geometry. By far, the largest effect was found in the press fit effect. In contrast to cracks which initiate directly at the press seat, cracks at geometrical transition grow much faster at the beginning which causes a detrimental reduction in residual lifetime. This can be accounted for by the magnification of the local mean load due to the press fits which is comparable to a residual stress effect, i.e., it does not affect the ΔK but the R ratio. A similar but smaller effect of the press fit was found by [18] investigating another axle's geometry. It has to be emphasised that the press fit effect is significant for any damage tolerance analysis of those types of components since its disregard would cause severe over-prediction of the residual lifetime.

Acknowledgement

M. Madia is a PhD student at Politecnico di Milano, Department of Mechanical Engineering, and this activity was mainly developed during his visits to GKSS Research Centre. This activity has been co-supported by a WIDEM EU Grant through which a research unit headed by Prof. F. Resta (Politecnico di Milano, Department of Mechanical Engineering) is involved.

The authors express their gratitude to Lucchini Sidermeccanica, especially to Mr. S. Cervello, for disclosing drawings of the locomotive axle analysed in the present research.

References

[1] Smith RA, Hillmansen S. A brief historical overview of the fatigue of railway axles. In: Proc Instn Mech Engrs. 2004; 218:267-277.
[2] Hirakawa K, Toyama K, Kubota M. The analysis and prevention of failure in railway axles. Int J Fatigue. 1998; 20(2):135-144.
[3] Zerbst U, Vormwald M, Andersch C, Mädler K, Pfuff M. The development of a damage tolerance concept for railway components and its demonstration for a railway axle. Eng Fract Mech. 2005; 72:209-239.
[4] Zerbst U, Mädler K, Hintze H. Fracture mechanics in railway applications - an overview. Eng Fract Mech. 2005; 72:163-194.
[5] Hillmansen S, Smith RA. The management of fatigue crack growth in railway axles. In: Proc Instn Mech Engrs. 2004; 218:327-336.
[6] Beretta S, Carboni M. Experiments and stochastic model for propagation lifetime of railway axles. Eng Fract Mech. 2006; 73:2627-2641.
[7] Carpinteri A, Brighenti R. Part-through cracks in round bars under cyclic combined axial and bending loading. Int J Fatigue. 1996; 18(1):33-39.
[8] Carpinteri A, Brighenti R, Spagnoli A. Surface flaws in cylindrical shafts under rotary bending. Fatigue Fract Engng Mater Struct. 1998; 21:1027-1035.
[9] Shiratori M, Miyoshi T, Sakay Y, Zhang GR. Analysis and application of influence coefficients for round bar with a semi-elliptical surface crack. In: Handbook of stress intensity factors, vol. II. Pergamon Press; 1987. p. 659-665.
[10] Carpinteri A, Brighenti R, Spagnoli A. Part-through cracks in pipes under cyclic bending. Nuclear Engng Design. 1998; 185:1-10.
[11] Carpinteri A, Brighenti R, Vantatori S. Surface cracks in notched round bars under cyclic tension and bending. Int J Fatigue. 2006; 28:251-260.
[12] EN 13104. Railway applications – Wheelsets and bogies – Powered axles – Design method. CEN. 2001.
[13] De Freitas M, François D. Analysis of fatigue crack growth in rotary bend specimens and railway axles. Fatigue Fract Engng Mater Struct. 1995;18(2):171-178.
[14] Beretta S, Carboni M. Rotary vs. plane bending for crack growth in railway axles. In: ESIS-TC24 meeting. Geesthacht, Germany, 2005.
[15] Lin XB, Smith RA. Shape evolution of surface cracks in fatigued round bars with semicircular circumferential notch. Int J Fatigue. 1999; 21:965-973.
[16] Lin XB, Smith RA. Fatigue growth simulation for cracks in notched and unnotched round bars. Int J Mech Sci. 1998; 40(5):405-419.
[17] Beretta S, Madia M, Schödel M, Zerbst U. In: Proceedings of the16th European Conference on Fracture. Alexandropolis, Greece, 2006.
[18] Zerbst U, Schödel M. Unpublished results.
[19] ABAQUS®. Ver 6.5.3 Reference Manual. 2005.
[20] Murakami Y. Metal Fatigue: Effects of Small Defects and Nonmetallic Inclusions. Oxford: Elsevier, 2002.
[21] Beretta S, Ghidini A, Lombardo F. Fracture mechanics and scale effects in the fatigue of railway axles. Eng Fract Mech. 2005; 72:195-208.
[22] Brocks W, Scheider I. Reliable J-values. MP Materialprüfung. 2003; 6:264-275.

[23] Newman Jr JC. A crack opening stress equation for fatigue crack growth. Int J Fracture. 1984; 24(4):R131-135.
[24] NASGRO. Reference Manual. Website: www.nasgro.swri.org. 2001.
[25] Newman Jr JC. A crack closure model for predicting fatigue crack growth under aircraft spectrum loading. Methods and models for predicting fatigue crack growth under random loading, vol. 784. ASTM STP; 1981. p. 53-84.